REPORT DOCUMENTATION PAGE

Form Approved
OMB No. 0704-0188

PLEASE DO NOT RETURN YOUR FORM TO THE ABOVE ORGANIZATION.

1. REPORT DATE *(DD-MM-YYYY)*	2. REPORT TYPE	3. DATES COVERED *(From - To)*
03-20-2008	Final	01/01/06 - 12/31/07

4. TITLE AND SUBTITLE
Advanced Transmission Electron Microscopy Characterization of Novel Thermoelectric Materials

5a. CONTRACT NUMBER

5b. GRANT NUMBER
N00014-06-1-0358

5c. PROGRAM ELEMENT NUMBER

6. AUTHOR(S)
Drs. Susanne Stemmer and John Bowers

5d. PROJECT NUMBER

5e. TASK NUMBER

5f. WORK UNIT NUMBER

7. PERFORMING ORGANIZATION NAME(S) AND ADDRESS(ES)
The Regents of the University of California
Office of Research
Cheadle Hall, Room #3227
Santa Barbara, CA 93106-2050

8. PERFORMING ORGANIZATION REPORT NUMBER

9. SPONSORING/MONITORING AGENCY NAME(S) AND ADDRESS(ES)
Office of Naval Research
875 North Randolf Street
Arlington, VA 22203-1995

10. SPONSOR/MONITOR'S ACRONYM(S)
ONR

11. SPONSOR/MONITOR'S REPORT NUMBER(S)

12. DISTRIBUTION/AVAILABILITY STATEMENT

DISTRIBUTION STATEMENT A
Approved for Public Release
Distribution Unlimited

13. SUPPLEMENTARY NOTES

14. ABSTRACT

The report described out research activities focused on the characterization of new epitaxial thermoelectric materials that are comprised of semimetallic, epitaxial ErAs nanoparticles embedded in a semiconducting epitaxial In0.53Ga0.47As (InGaAs) matrix. The composites were grown by molecular beam epitaxy. We used advanced transmission electron microscopy (TEM) techniques to perform a detailed analysis of the shapes and distribution of random ErAs particles and the overall morphology of the composites. We show that the size of the particles is relatively insensitive to most growth parameters, except for the growth temperature and matrix (GaAs or InGaAs). We found that particles tend to order in specific crystallographic planes. We discuss the mechanism leading to the ordering. We also report on the characterization of epitaxial ScN/Zr(W)N superlattices for thermoelectric applications.

15. SUBJECT TERMS
Thermoelectric materials, microstructure characterization

16. SECURITY CLASSIFICATION OF:			17. LIMITATION OF ABSTRACT	18. NUMBER OF PAGES	19a. NAME OF RESPONSIBLE PERSON
a. REPORT	b. ABSTRACT	c. THIS PAGE			Dr. Susanne Stemmer
U	UU	U	SAR	15	19b. TELEPHONE NUMBER *(Include area code)* 805.893.6128

Contract Information

Contract Number	N00014-06-1-0358
Title of Research	Advanced Transmission Electron Microscopy Characterization of Novel Thermoelectric Materials
Principal Investigator	John Bowers, Susanne Stemmer
Organization	University of California, Santa Barbara

Technical Section

Technical Objectives

Research activities focused on the characterization of new epitaxial thermoelectric materials that are comprised of semimetallic, epitaxial ErAs nanoparticles embedded in a semiconducting epitaxial $In_{0.53}Ga_{0.47}As$ (InGaAs) matrix. Prior work in the ONR funded MURI "Thermionic Energy Conversion Center" had shown that the power factor of randomly distributed ErAs in $In_{0.53}Ga_{0.47}As$ was slightly higher than that of $In_{0.53}Ga_{0.47}As$ and that the thermal conductivity was reduced by almost a factor of two below the alloy limit. The resulting *ZT* is increased more than a factor of two. Furthermore, theoretical work in the MURI had shown that ErAs particles scatter in the long to midrange wavelength phonons and that a large distribution of sizes is advantageous for thermal conductivity reduction.

The goal of the transmission electron microscopy (TEM) characterization effort in this program is to perform a detailed analysis of the shapes and distribution of random ErAs particles and the overall morphology of the composites. The ultimate goal is to determine the growth parameters that yield optimized thermoelectric performance of these novel composites.

In addition, TEM studies also focused on the characterization of (Zr,W)N/ScN superlattices. These metal/semiconductor superlattices were shown to have thermal conductivities below 4 W/m-K, also as part of the ONR MURI (Prof. T. Sands).

Technical Approach

ErAs nanocomposites were grown in Prof. Art Gossard's group at UCSB by molecular beam epitaxy by graduate student Josh Zide. The matrix in which the ErAs particles were embedded consisted of either lattice-matched $In_{0.53}Ga_{0.47}As$ (InGaAs) layers were grown on (001) semi-insulating InP:Fe, or epitaxial GaAs layers on GaAs. The erbium was co-deposited during $In_{0.53}Ga_{0.47}As$ or GaAs layer growth, respectively. The compositions reported here were calculated as a ratio of the growth rates of ErAs to InGaAs (in monolayers/second).

To investigate the influence of growth parameters on the composite structure, the following growth parameters were varied:

- Er-concentration (0.3% - 6%)
- Layer growth temperature
- Growth rate

- Matrix composition ($In_{0.53}Ga_{0.47}As$ or GaAs)

Plan-view and cross-section TEM samples were prepared along two perpendicular crystallographic directions, namely $[001]_{InGaAs}$ and $[110]_{InGaAs}$. Conventional TEM bright-field (BF) and dark-field (DF) diffraction contrast imaging was used to study particle distributions over large areas and to determine the uniformity of the shape distribution, because large areas could be imaged with conventional TEM. The disadvantage of DF images is that the contrast varies across the image to changes in the diffraction conditions. Therefore, HRTEM and HAADF/STEM images were used for detailed analysis of the size of the particles. Both techniques allow for atomic resolution analysis.

The TEM work was carried out by Dr. Dmitri Klenov, a postdoctoral researcher in Prof. Stemmer's group at UCSB, by Mr. James LeBeau, a graduate student in the same group and by Dr. Joel Cagnon, a postdoc in the same group. Table I lists the TEM techniques employed in this work.

Technique	Acronym	Capabilities and Purpose
High-angle annular dark-field (HAADF) imaging in scanning transmission electron microscopy (STEM)	HAADF/STEM	Atomic number sensitive, atomic resolution structure of particles and interfaces
Bright Field/Dark Field Imaging in Conventional TEM	BF/DF	Distribution of particles
High-resolution transmission electron microscopy	HRTEM	Detailed particle shape analysis

The rock salt metal/semiconductor superlattices were grown by Prof. Tim Sands group at Purdue University. The TEM work was carried out by Dr. Joel Cagnon, a postdoc in Prof. Stemmer's group.

Technical Results

ErAs Particle Shapes and Sizes

ErAs particle sizes and shapes were characterized using selected HRTEM or HAADF/STEM images. The ErAs particles perimeters were outlined using image processing software (ImageTool 4.0). To account for the anisotropy in the ErAs particle shapes, particle sizes were characterized by measuring their length along their longest axis ("major axis") and in the direction perpendicular to it ("minor axis").

Figure 1(a) shows DF image of a plan-view sample. The ErAs particles appear bright in this image. For comparison a HRTEM image acquired from the same region is shown in Fig. 1(b).

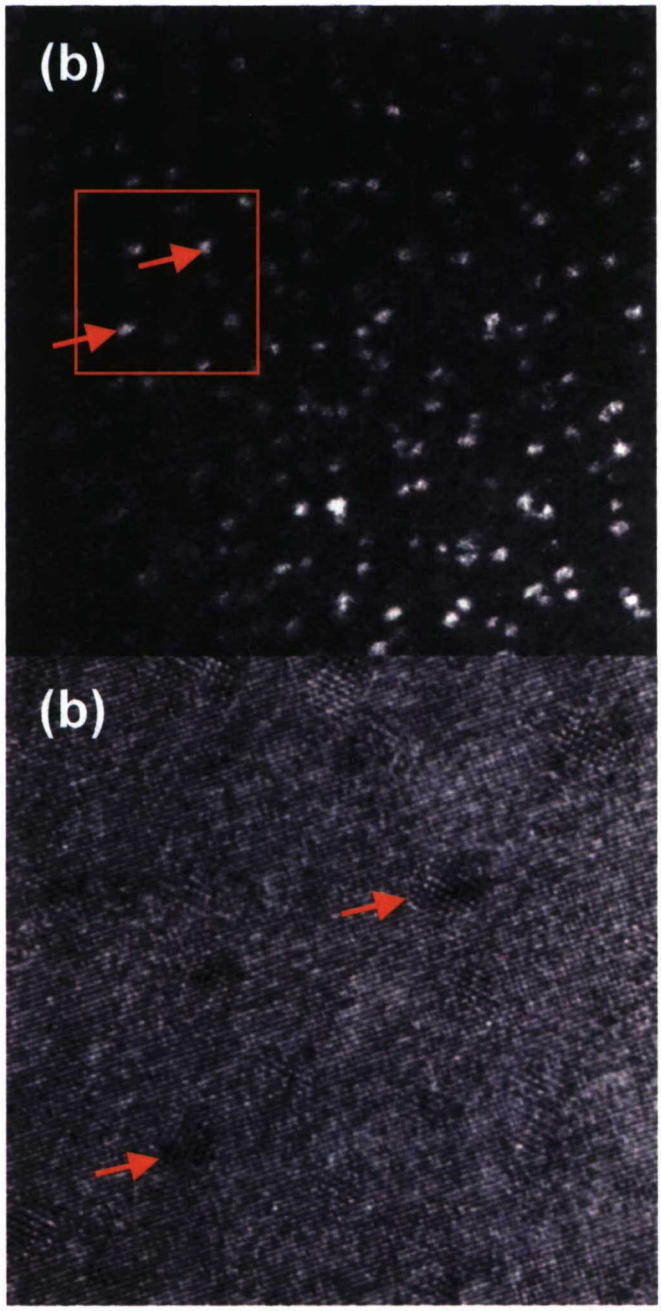

Figure 1: Dark-field plan-view image of a sample with 3% ErAs in InGaAs. (b) Section of the corresponding HRTEM image. A few ErAs particles are indicated by red arrows.

Figure 2 shows a plan-view HRTEM image of the particles in a sample with 3% ErAs. Shown in the inset are the particles that are visible in this image outlined and filled with black ink. As can be seen from Fig. 2, the ErAs particles were distributed uniformly and their sizes varied only within a narrow range of a few nanometers. Some of the particles were coalesced so that the length of the structure was doubled (or tripled).

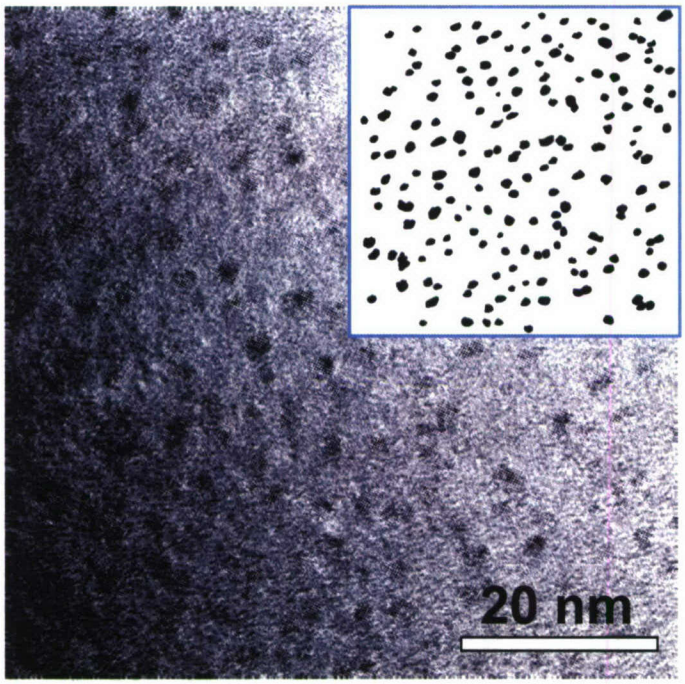

Figure 2: Plan-view HRTEM image of ErAs particles in InGaAs (3 % sample). The inset shows the particle distribution.

Figure 3 shows histograms of the ErAs particle length distributions along the long axis (a-b) and the direction perpendicular to it (c-d). Particle sizes ranged between 1 nm and 3.5 nm. A few particles with larger lengths were formed by coalescence. The ErAs particles were somewhat anisotropic in shape. In particular they were elongated along one of the $[1\bar{1}0]$ directions, which is the fast diffusion direction in InGaAs, as seen from the polar histograms shown in Figs. 3(b) and 3(d). Most of the longer axes of the ErAs particles were close to $[1\bar{1}0]$, while the perpendicular axes were mostly oriented along [110]. This finding was similar to what was observed previously in ErAs nanoparticle superlattices [1, 2].

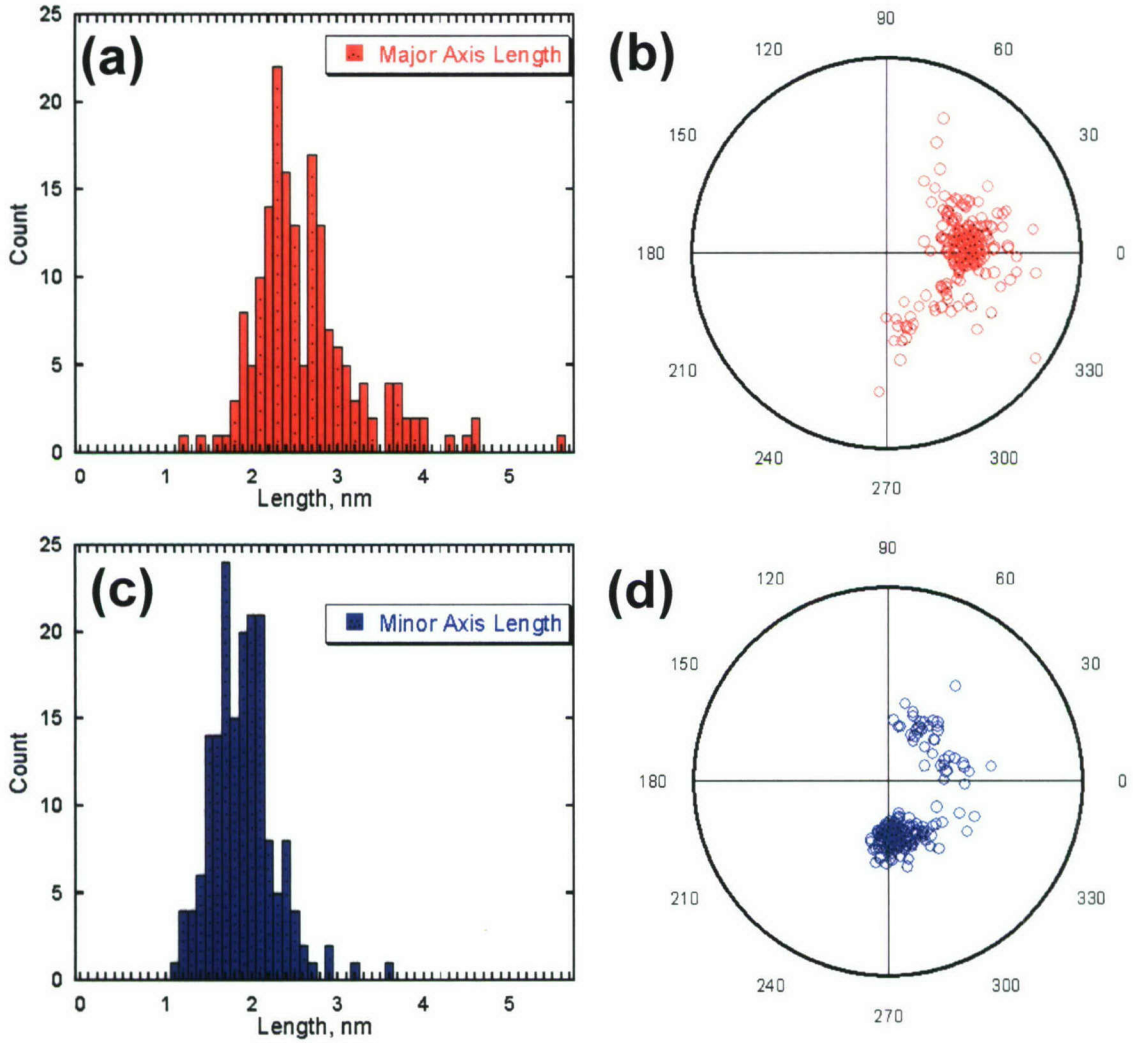

Figure 3: Histograms showing the particle size distribution in a plan-view sample with 3% ErAs. (a) and (c) show the particle length measured along the major (long) and minor (perpendicular) axes, respectively. (b) and (d) show the angles between the two particle axes and the [110] direction of InGaAs.

Figure 4 shows a HAADF/STEM cross-section image of the sample. The ErAs particles show similar distribution as in plan-view, although fewer coalesced particles were observed. The particle size distribution was also similar as in plan-view (Fig. 5). The particle sizes vary from 1.2 nm to 3.2 nm with fewer particles with larger sizes compared to the plan-view sample. The particles did not show pronounced elongation along a specific axis of InGaAs [Figs. 5(c) and 5(d)]. As a result, the distribution was slightly narrower than in plan-view.

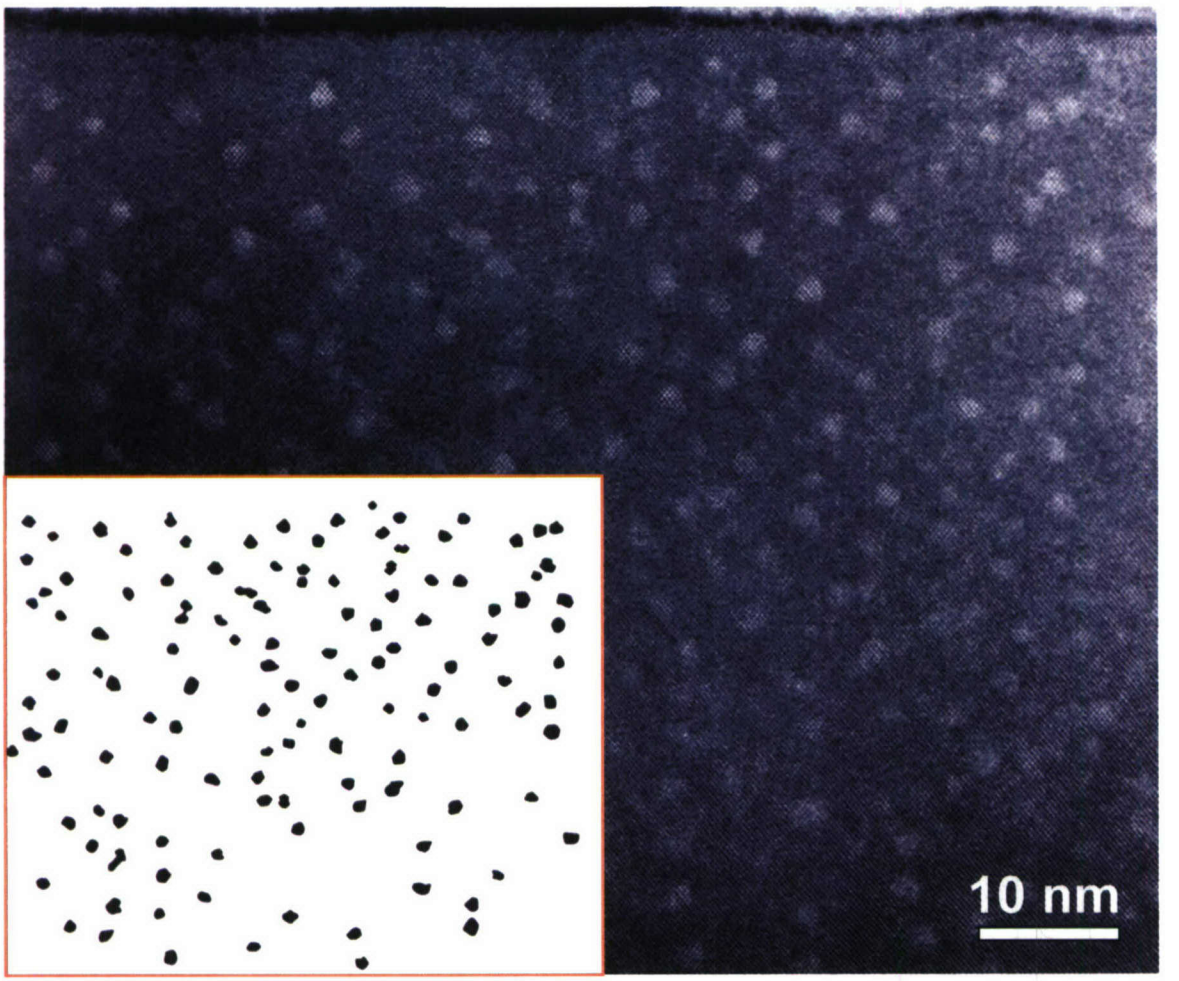

Figure 4: Cross-section HAADF-STEM image of ErAs particles (3% sample) in InGaAs. The inset shows the particle distribution obtained from this image. The ErAs particles appear bright because of the strong atomic number contrast of this technique.

In summary, ErAs particles in a random 3% ErAs sample were found to have an elliptical shape with the longer axis parallel to the $[1\bar{1}0]$ fast-diffusion direction in InGaAs. The particle sizes varied from 1 to 3.5 nm, with some of the particles having longer lengths (up to approximately 10 nm) due to coalescence during growth.

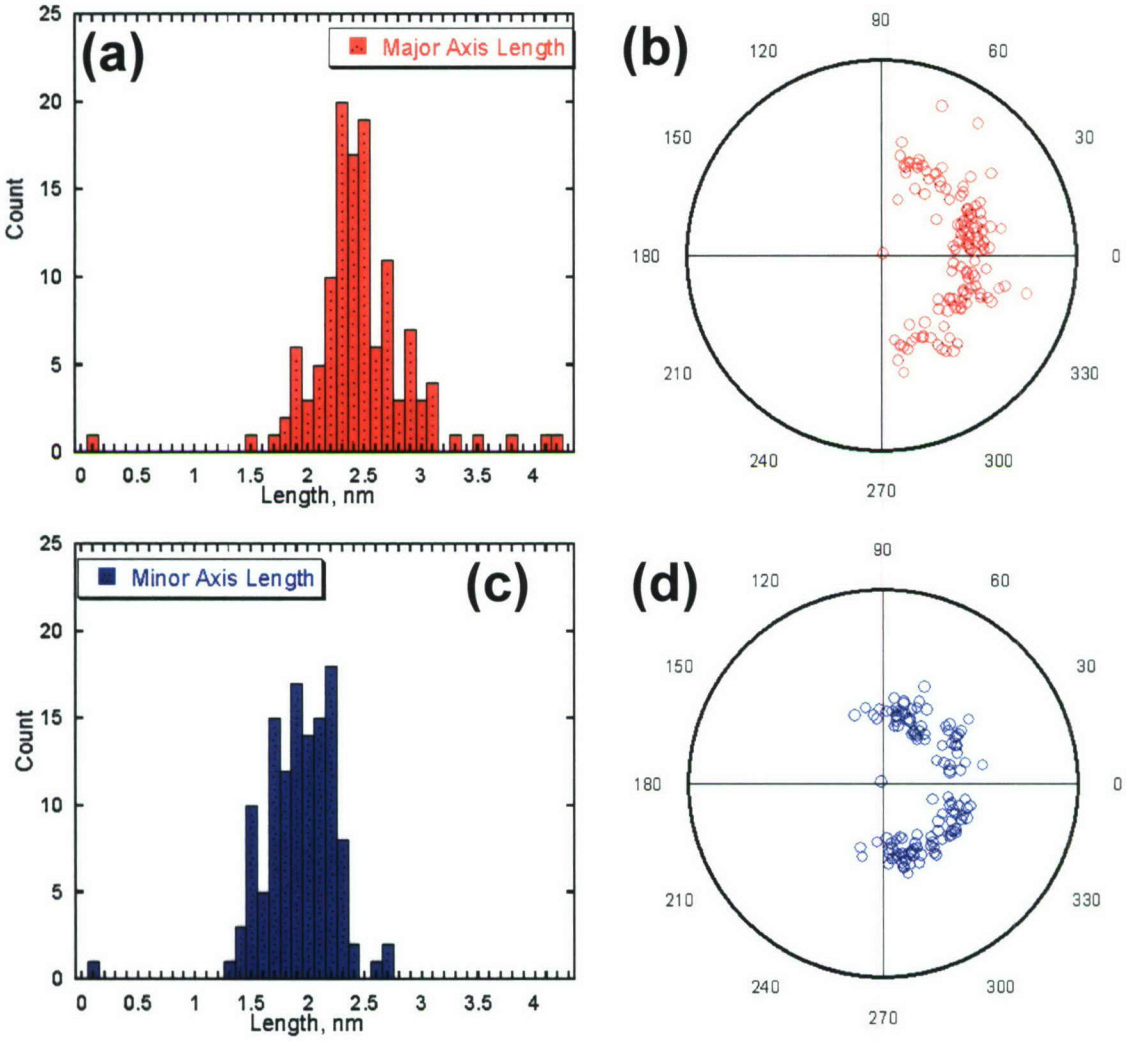

Figure 5: Histograms showing the particle size distribution in a cross-section sample with 3% ErAs. (a) and (c) show the particle length measured along the major (long) and minor (perpendicular) axes, respectively. (b) and (d) show the angles between the two particle axes and the [110] direction of InGaAs.

A second goal was to provide an understanding of the the impact of the growth conditions on the particle size distributions. In particular, the influence of the amount of deposited Er during InGaAs growth was studied. Towards this goal a multilayer sample was deposited, which consisted of 4 layers of 100 nm InGaAs with different amount of ErAs. The Er-containing layers are separated by 20 nm of pure InGaAs followed by 2 nm of InAlAs. Figure 6 shows a cross-section HAADF-STEM image of this sample.

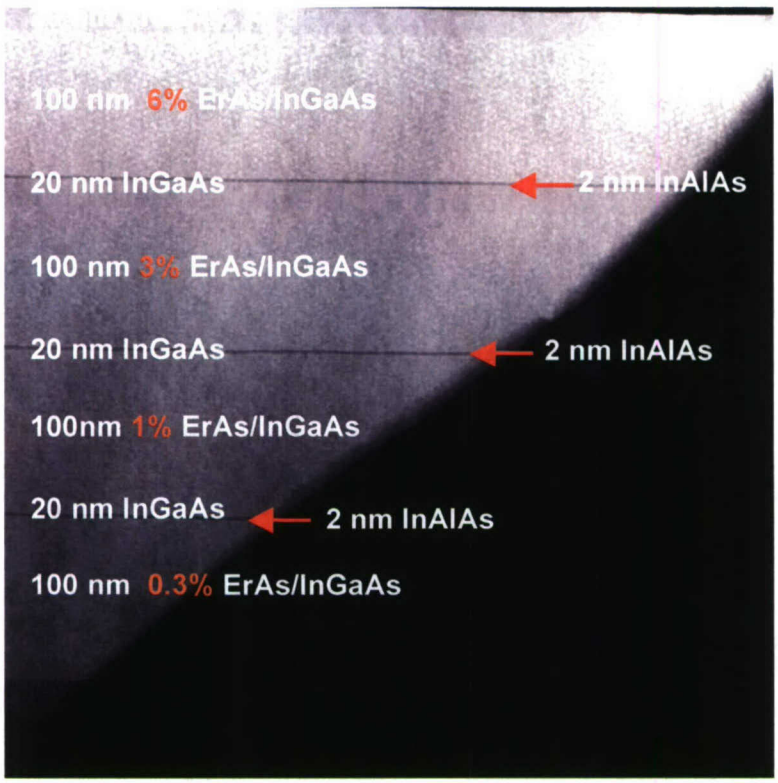

Figure 6: Cross-section HAADF-STEM image of the sample with different amount of random ErAs particles. The amounts of ErAs are indicated. Note the spacer layers between the Er-containing layers. The ErAs particles appear bright because of the strong atomic number contrast of this technique.

A qualitative comparison of the particle distribution (Fig. 7) did not show significant differences in the particle sizes in layers containing different amounts of ErAs. Increasing amounts of Er incorporation during growth mainly resulted in a higher density of the particles. Higher particle densities also resulted in more particles that were coalesced; as a result, layers with more than 3% ErAs had more elongated particles with larger lengths. Furthermore, the thickness of the InGaAs layers containing ErAs increased with the increasing amounts of Er.

An unexpected result obtained from this sample was the observation of long-range ordering of ErAs particles in layers with higher densities of ErAs (Fig. 7), discussed below.

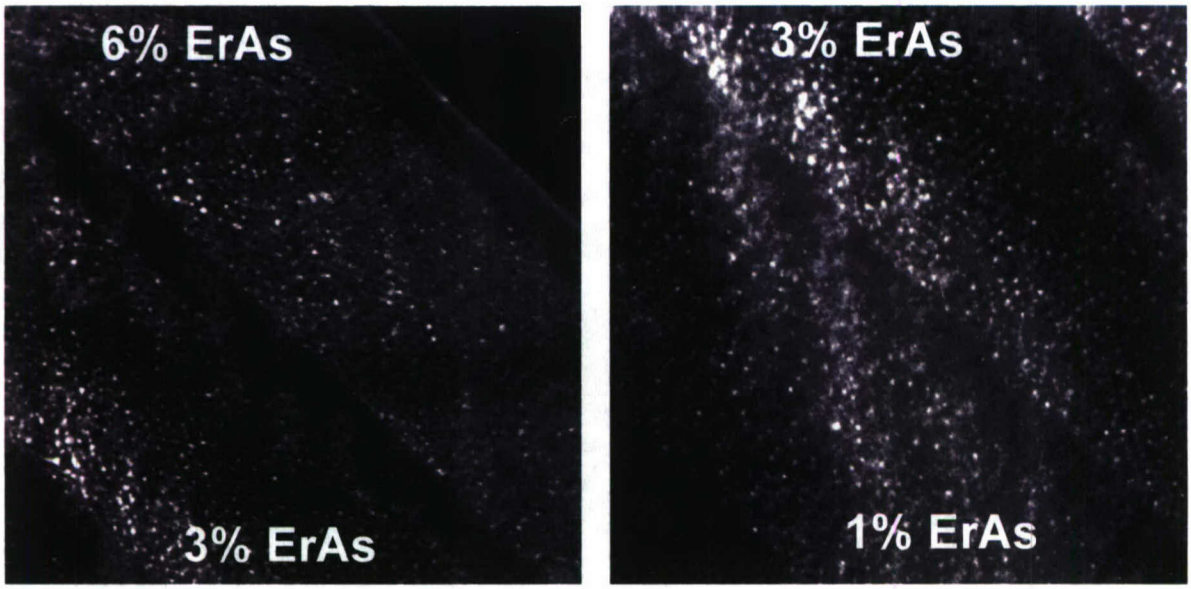

Figure 7: DF images of the InGaAs with 6%, 3% and 1% of ErAs recorded from the multilayer sample shown in Fig. 6. The particles appear bright in this technique. Note the ordering of particles in the 3% and 6% layers.

ErAs Particle Ordering

Composites with higher concentrations of Er showed ordering of particles in the InGaAs matrices. This was further investigated in the present project period. Figure 8 shows a low-magnification, conventional dark-field image of the sample containing $In_{0.53}Ga_{0.47}As$ layers with increasing amounts of Er. The ErAs particles appeared bright in this image. At higher concentrations of Er the density of the particles increased, but their shapes and sizes (1 – 3 nm) were approximately independent of their density. Figure 8a shows a cross-sectional HAADF/STEM image recorded along one of the <110> directions of the sample containing $In_{0.53}Ga_{0.47}As$ layers with 6% ErAs. The strong atomic number sensitivity in HAADF imaging caused the ErAs particles to appear bright. Along this direction, particles showed strong ordering. In particular, particles were preferentially located in the $\{114\}_{InGaAs}$ planes, at an angle of ~ ±19° with the (001) surface. Some preference also existed for the particles to be located near the intersection of the cross-grid formed by the $\{114\}_{InGaAs}$ particle planes (see schematic in Fig. 9), which caused the columnar stacking of the particles parallel to the growth direction in many regions. The inset in Fig. 8a shows a Fourier transform (FT) of the image. The streaked, strong reflections in the FT corresponded to the ordering in $\{114\}_{InGaAs}$ planes. The average spacing of the planes containing the particles was about 4 nm. The FT also confirmed the stacking parallel to the growth direction (note the weak intensity maxima in the horizontal direction). A cross-section image recorded along the <110> direction perpendicular to that shown Fig 8a demonstrates an absence of ErAs particle ordering (Fig. 8b) and shows no discrete features due to the particles. This could be explained with anisotropy in the ordering with particles lining up in channels along the first <110> direction. Preferential growth along one of

the <110> directions is commonly observed in ErAs/InGaAs superlattice structures due to anisotropy in surface diffusion, which is much faster along $[\bar{1}10]$. Furthermore, discrete rows of particles could not be seen in Fig. 1b because of deviations from the positions exactly at the intersections of the $\{114\}_{InGaAs}$ particle planes combined with the high density of the particles (note that the spacing was less than a typical TEM foil thickness). Figure 9 shows a schematic model of the observed ordering deduced from the images in Fig. 8.

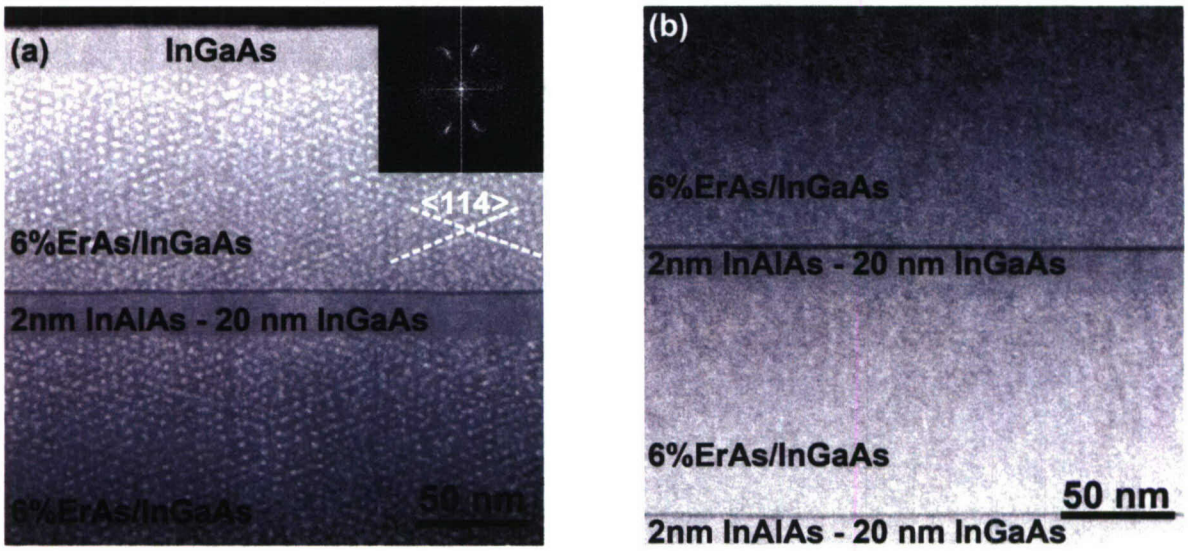

Figure 8: (a) Cross-sectional HAADF/STEM image along one of the <110> directions of the top two layers of the sample with 6% ErAs. The inset is a Fourier transform of the image. (b) Cross-sectional HAADF/STEM image in the perpendicular <110> direction.

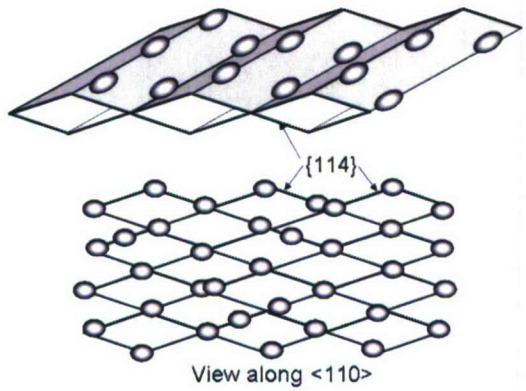

Figure 9: Schematic model of the ordering of ErAs particles in InGaAs layers. The viewing direction in Fig. 9a is parallel to the channels and perpendicular to them in Fig. 9b. The ErAs particles show a strong preference for being located on $\{114\}_{InGaAs}$ planes and a somewhat less pronounced preference for being located exactly in the troughs and peaks (i.e. the intersections of these planes).

It is likely that during co-deposition, particles formed on the surface of the growing film and not via precipitation from the bulk. The size of the particles was independent of their density, possibly because further growth was limited by diffusion after the particles became embedded in the InGaAs matrix.

Several possible reasons may account for the observed ordering of ErAs nanoparticles in a semiconductor matrix, including interaction of the particles via anisotropic lattice strain surrounding the particles or electrostatic forces. A third possibility included the formation of the ErAs particles on a facetted InGaAs growth surface. For example, the Er may have caused an InGaAs surface instability by modifying the surface energies. RHEED during growth of a 6% layer showed chevrons along <110>, indicative of facets. The surface of the Er-containing layers appeared to be corrugated (see Fig. 1a), whereas the InGaAs without Er had flat surfaces. It should be noted that if ErAs particles grew on a facetted growth surface, subsequent perturbations were periodically out-of-phase (see Fig. 9).

In addition to surface energy anisotropy, InGaAs surfaces are known to facet parallel to (114) to accommodate misfit stresses with the substrate. While the $In_{0.53}Ga_{0.47}As$ was lattice matched to InP, incorporation of Er atoms or ErAs particles may have caused the layer to become mismatched. However, this was not believed to be the origin for the observed ordering, because the layers with different amounts of Er (3% and 6%) showed a similar pattern of ordering. Furthermore, ErAs particles embedded in epitaxial GaAs layers grown on GaAs crystals showed a very similar pattern of ordering in {114} planes along one of the <110> directions, with a similar spacing of ~ 4 nm. In contrast to $In_{0.53}Ga_{0.47}As$, GaAs has a smaller lattice parameter than ErAs. Therefore, one may speculate that the observed ordering was either due to short-range interactions between the ErAs particles themselves or a surface instability driven by Er. Further experiments are planned to distinguish between the different possible mechanisms of ordering.

Influence of Growth Parameters on ErAs Particle Size and Spacing

Varying the Er concentration (between 0.3 and 6 % Er) had little influence on the particle size and shapes. Similarly, we found that changing the growth rate between 0.25 μm/hr and 1.25 μm/hr had no significant influence on the particle size. This is advantageous, as for thermoelectric applications thick layers and thus high growth rates are likely required.

We also investigated the growth temperature dependence of both GaAs and InGaAs matrices. A typical sample with layers grown at different temperatures is shown in Fig. 10. The bottom layers were "annealed" at higher temperatures during the growth of the upper layers. Thus any change in particles size due to longer exposures at high temperatures, as might be relevant for applications, could also be monitored. In addition to particle sizes, particle spacings are reported. This corresponds to the projected spacing of the {114} particle containing planes obtained from Fourier transforms of the images.

For both InGaAs and GaAs, the particle size and spacing was found to depend on the growth temperature (see Tables I and II). No significant change in the particles sizes was observed as a result of the annealing of the bottom layers, indicating that these composites are

likely stable during application. The particles showed ordering in {114} planes, independent of growth temperature and matrix. The particles were larger in InGaAs than in GaAs.

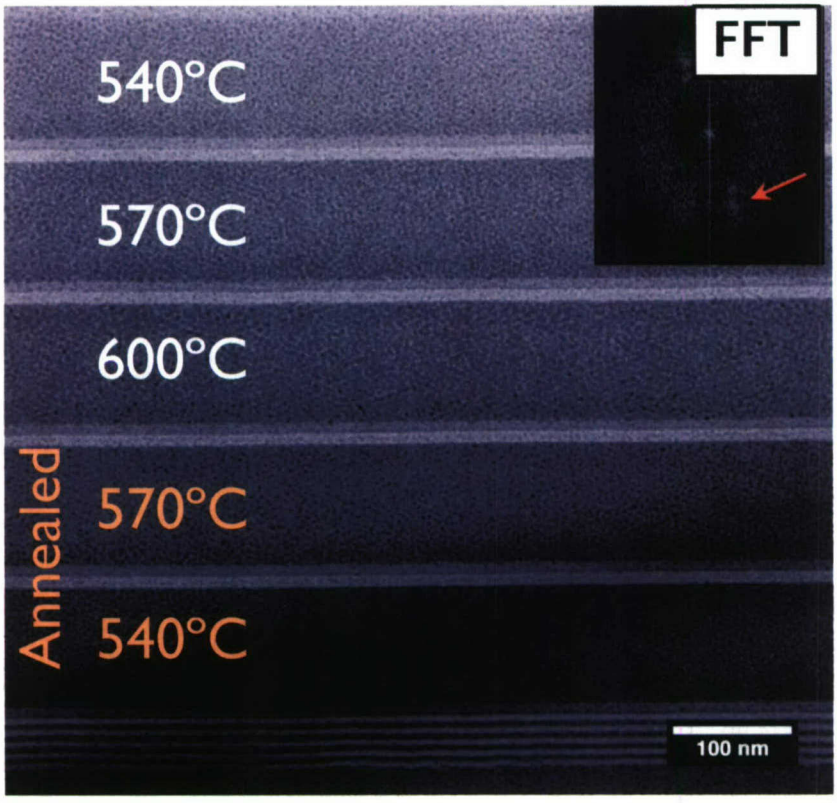

Figure 10: Conventional bright-field image (particles appear dark) of GaAs layers with 1% Er and a growth rate of 1 μm/hr. The growth temperatures are indicated. The inset shows a Fourier transform of the image. The peaks in the Fourier transform are due to particle ordering in {114} planes, described above.

Table I: Growth temperature dependence of particles sizes (measured area) and particle spacings for ErAs: GaAs composites.

Growth Temperature (°C)	Average Size (nm^2)	Particle Spacings {114} (nm)
Annealed		
540	2.5±.5	4.1
570	2.4±.5	4.5
Non-Annealed		
600	3.3±.6	5.4
570	2.6±.4	4.5
540	2.2±.5	4.1

Table II: Growth temperature dependence of particles sizes (measured area) and particle spacings for ErAs: InGaAs composites.

Growth Temperature (°C)	Average Size (nm^2)	Particle Spacings {114} (nm)
Annealed		
400	1.9±.3	3.6
450	2.5±.6	3.8
Non-Annealed		
500	4.7±1.0	5.2
450	2.8±.5	3.8
400	1.9±.5	3.6

Microstuctures of Rock Salt Superlattices

The TEM studies of (Zr,W)N/ScN superlattices grown in Prof. Sands group at Purdue were carried out to address the following questions:

- Are (Zr,W)N/ScN interfaces coherent (ZrN was alloyed with WN to improve the lattice mismatch with ScN)?
- What are the defect densities?
- What is the homogeneity of the (Zr,W)N alloy (important for alloy scattering)?

Figure 11 shows a schematic of the sample that was received from Prof. Sands.

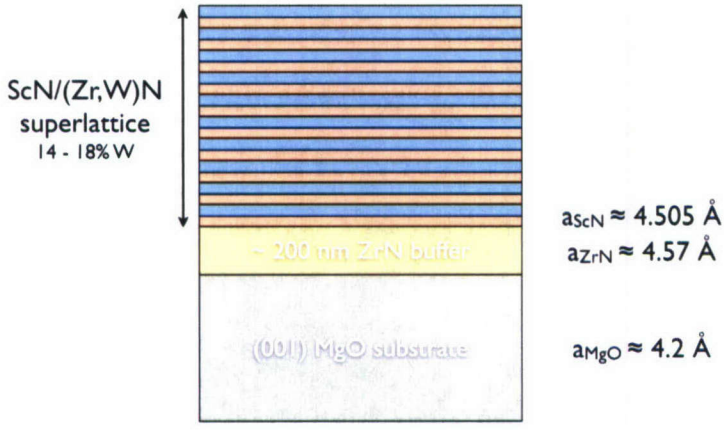

Figure 11: Schematic of the rock salt superlattice sample.

Figure 12 shows a low magnification cross-section bright-field image of the sample. It shows that the superlattice contains a high density of extended defects, mostly threading dislocations. The density is highest in the ZrN buffer layer and decreases towards the film surface. This is likely due to dislocation reactions. Occasionally the surface contained pits, which did not reach through the entire film thickness.

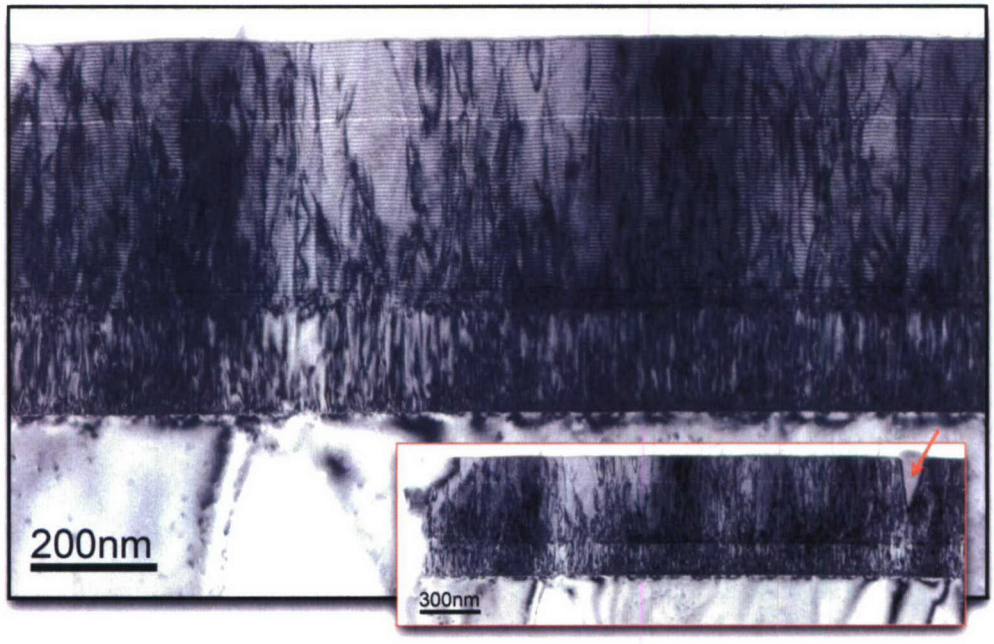

Figure 12: Schematic of the rock salt superlattice sample.

High-resolution HAADF imaging (Fig. 13) showed that the layers of Zr(W)N and ScN had somewhat different thicknesses, which is due to different growth rates. Epitaxial growth throughout the superlattice was observed. All the layers showed coherent interfaces. No long range order was observed in the (Zr,W)N alloy, although short range order cannot yet be excluded. Furthermore, "bending" of the layers near threding dislocations was observed. This was likely due to the formation of surface pits near the dislocations.

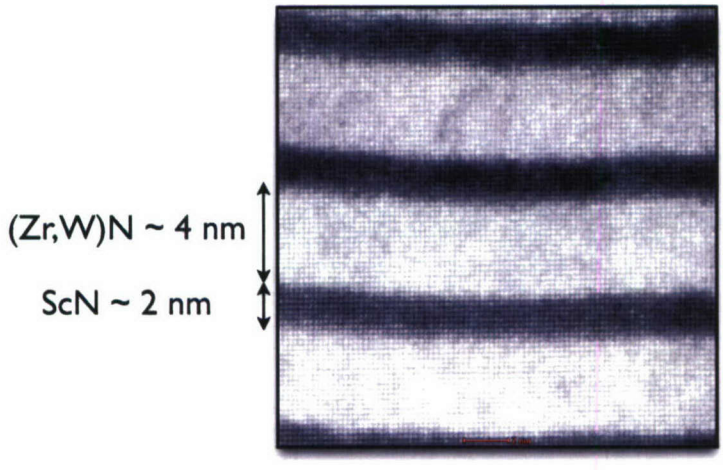

Figure 13: Atomic resolution HAADF images of a layer sequence. The (Zr,W)N alloy is brighter because of its higher atomic number.

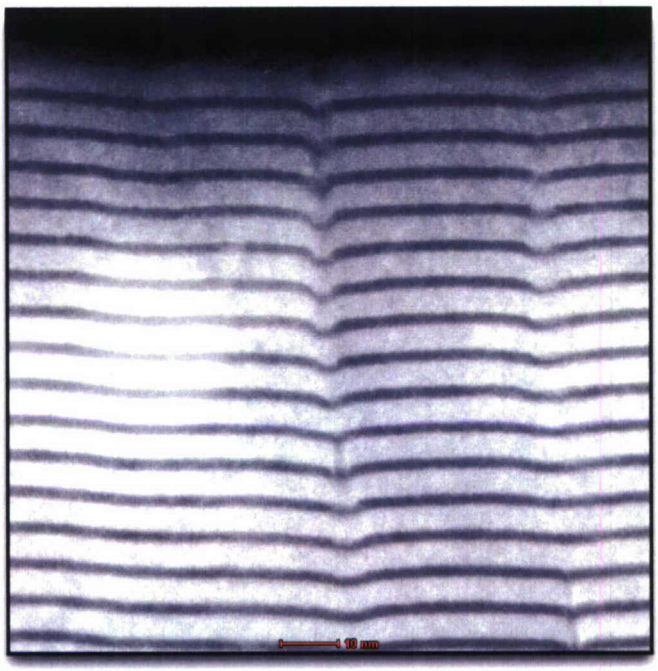

Figure 14: Low resolution HAADF image of the superlattice layers, showing "bending" near threading dislocations.